Web-post buckling resistance for perforated high-strength steel beams with elliptically-based web openings

Felipe Piana Vendramell Ferreira[a]*, Rabee Shamass[b], Luis Fernando Pinho Santos[b], Konstantinos Daniel Tsavdaridis[c], Vireen Limbachiya[b]

[a]Federal University of Uberlândia, Faculty of Civil Engineering – Campus Santa Mônica, Uberlândia, Minas Gerais, Brazil

[b]London South Bank University, School of Built Environment and Architecture, London, UK

[c]Department of Engineering, School of Science and Technology, City, University of London, Northampton Square, EC1V 0HB, London, UK

**Corresponding author*

Abstract

There has been an increase in the use of high-strength steel in several countries, as they provide design lightweight structural members by satisfying environmental and economic issues. This paper aims to implement high-strength steels in the web-post buckling resistance equation, which was based on the truss model according to EUROCODE 3, presented previously by the authors. For this task, a finite element model is developed by geometrically and materially nonlinear analysis with imperfections included. A parametric study is carried out, considering the key geometric parameters that influence the web-post buckling resistance. Three high-strength steel grades are studied (S460, S690 and S960) and in total, 13,500 finite element models are processed. A new factor for adapting high-strength steels to the equation proposed previously was presented. The finite element results agree well with the new proposal. The statistical parameters calculated, via the ratio between the numerical and analytical models, considering the regression, mean, standard deviation and variance, were 0.9817, 0.986, 8.32% and 0.69%, respectively. In conclusion, a reliability analysis was presented based on Annex D EN 1990 (2002).

Keywords: High-strength steel; Elliptically-based web openings; Finite element method; Web-post buckling; Reliability analysis.

E-mail addresses:
fpvferreira@ufu.br (F. P. V. Ferreira)
shamassr@lsbu.ac.uk (R. Shamass)
pinhosl3@lsbu.ac.uk (L. F. P. Santos)
konstantinos.tsavdaridis@city.ac.uk (K. D. Tsavdaridis)
limbachv@lsbu.ac.uk (V. Limbachiya)

Notation

The following notations and symbols are used in this paper:

b_f	the flange width;	k	Coefficient in Eq. (2);
d	the parent section height;	K	Coefficient in Eq. (9);
d_g	the total height after castellation process;	K_{HSS}	Coefficient in Eq. (13);
d_o	the opening height;	l_{eff}	the web-post effective length;
d_t	the tee height;	R	the opening radius;
$f_{cr,w}$	the critical shear stress in the web-post;	s	the web-post width;
f_y	the yield strength of the steel section;	t_f	the flange thickness;
f_u	the ultimate stress of the steel section;	t_w	the web thickness;
h	the distance between flanges geometric centres of the parent section;	V	the global shear;
H	the distance between flanges geometric centres after castellation process;	w	the opening width;
		ε	strain;
		λ_0	the reduced slenderness factor;
		λ_w	the web-post slenderness factor;
		σ	stress;
		χ	the reduction factor;

1. Introduction

Steel beams with elliptically-based periodical web openings are manufactured employing the castellation process (**Fig. 1**) and that leads to reduced steel waste and reduce energy spent in comparison to the perforated beams with circular openings due to the profile cutting. Moreover, this particular shape of web openings fosters the reposition of the stress concentration points (aka plastic hinges) nearer to the NA which also results to increased capacity. Overall, they present several advantages in construction buildings, highlighting the flexural stiffness due castellation process, the reduction in the structure's self-weight with the addition of multiple closely spaced periodical web openings, reduction in the structural floor height since the openings allow the passage of ducts for service integration and favors the flow of air in closed environments such as underground parking [1,2].

However, due to the presence of adjacent web openings and long spans, those beams can reach different buckling modes, i.e., lateral-torsional, web-post, web distortional, local flange and web, or even the interaction between them [3–6]. The present study focuses on the web-post buckling. It is a local web buckling mode with double curvature characterised by a lateral displacement with torsion due to the horizontal shear acting in the web-post [7,8]. In general, the main geometric parameters that influence the web-post buckling resistance of perforated beams are the opening height, the web-post width, and the web thickness [9,10].

Studies of steel beams with elliptically-based web openings started with Tsavdaridis [11] and subsequently, several results were published. Tsavdaridis and D'Mello [12,13] and Tsavdaridis et al. [14] worked with optimization problems considering various shapes of openings. These studies highlighted that elliptically-based web openings resisted the formation of plastic hinges at low values of loading. Tsavdaridis and D'Mello [8] carried out tests considering different web openings shapes. The beams were subjected to three-point bending. This investigation showed that elliptically-based web openings had greater resistance to horizontal shear which caused the web-post buckling. In Tsavdaridis and D'Mello [15], an optimisation study was conducted to assess the Vierendeel mechanism resistance. The authors emphasized that the elliptical-based web openings showed an increase in the flexural stiffness, i.e., lower deflections when compared to steel beams with circular web openings. Ferreira et al. [16] presented a web-post buckling resistance calculation procedure focused on EC3 [17] strut model. This procedure is presented in section 2.

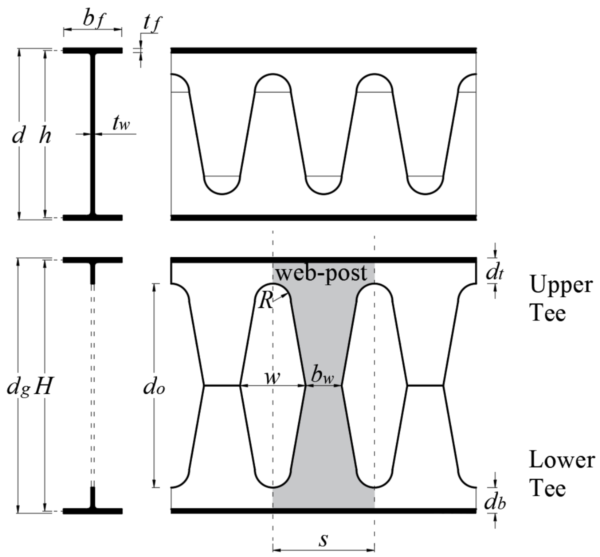

Fig. 1: Steel beams with elliptically-based web openings [18]

All previous studies employed normal strength steels, such as S275 and S355. High-strength steels (HSS) are those with a yield strength (f_y) greater or equal to 460 MPa. The application of HSS has been increasing in several countries, mainly due to economic and environmental issues, since less material is used to perform the same functions as normal strength steels, as well as possess an increased corrosion resistance leading to durability and low maintenance [19–24]. The application of HSS makes the design of lightweight structures possible by achieving substantial weight savings where 34% savings had been recorded [25]. This paper aims to investigate the web-post buckling resistance of steel beams with elliptically-based web openings made of HSS. For this task, a finite element model is developed and calibrated with tests by buckling and post-buckling analyses using Abaqus [26]. A parametric study is conducted considering three classes of high-strength steel, such as S460, S690 and S960. A Python script is written to automate the high volume of analyses and a total of 13,500 finite element models are developed. The results are discussed and a proposal is made for design focus.

2. Web-post buckling resistance of perforated steel beams with elliptically-based web openings

The calculation procedure, which is presented here, is based on the compressed truss model (**Fig. 2**), according to EC3 [17], considering buckling curves. In this scenario, SCI P355 [27] recommends using the buckling curves *b* and *c* for hot-rolled and welded sections, respectively. Although these recommendations are directed to perforated steel beams with circular web openings, it is possible to apply them to steel beams with elliptical-based web openings, since these structures are also manufactured by the castellation process (similar to cellular beams), taking into account thermal cutting and welding.

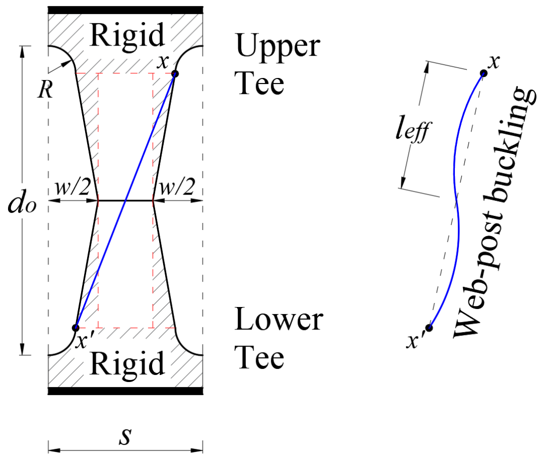

Fig. 2: Compressed truss model [16]

According to Ferreira et al. [16], the web-post buckling resistance is calculated considering **Eqs. (1-10)**, in which l_{eff} is the web-post effective length, do is the opening height, R is the opening radius, H is the distance between flanges geometric centres after castellation process, s is the web-post width, w is the opening height, λ_w is the the web-post slenderness factor, t_w is the web thickness, $f_{cr,w}$ is the critical shear stress in the web-post, f_y is the yield strength, λ_0 is the reduced slenderness factor and χ is the reduction factor. Although the web-post buckling resistance results presented by these equations were accurate in the previous study, it is important to highlight that high-strength steels had not been considered.

$$l_{eff} = k\sqrt{\left(\frac{d_o - 2R}{2}\right)^2 + \left(\frac{s}{2} - R\right)^2} \tag{1}$$

$$k = 0.516 - 0.288\left(\frac{H}{d_o}\right) + 0.062\left(\frac{s}{s-w}\right) + 2.384\left(\frac{s}{d_o}\right) - 2.906\left(\frac{w}{d_o}\right) \tag{2}$$

$$\lambda_w = \frac{l_{eff}\sqrt{12}}{t_w} \tag{3}$$

$$f_{cr,w} = \frac{\pi^2 E}{{\lambda_w}^2} \tag{4}$$

$$\lambda_0 = \sqrt{\frac{f_y}{f_{cr,w}}} \tag{5}$$

$$\phi = 0.5\left[1 + 0.49(\lambda_0 - 0.2) + {\lambda_0}^2\right] \tag{6}$$

$$\chi = \frac{1}{\phi + \sqrt{\phi^2 - {\lambda_0}^2}} \leq 1.0 \tag{7}$$

$$\sigma_{Rk} = K\chi f_y \tag{8}$$

$$K = -1.318 + 1.790\left(\frac{H}{d_o}\right) + 0.413\left(\frac{s}{s-w}\right) - 1.926\left(\frac{s}{d_o}\right) + 0.937\left(\frac{w}{d_o}\right) - 0.02\left(\frac{d_o}{t_w}\right) + 1.412\lambda_0 \tag{9}$$

$$V_{Rk} = \sigma_{Rk} t_w (s - w) \tag{10}$$

3. Finite element method

There are no tests available in the literature in relation to HSS beams with elliptically-based web openings. Hence, a numerical model is developed and validated for beams made of normal strength steel, such as S355 grade. In this context, A1, A2, B1, B2 and B3 tests, which were carried out by Tsavdaridis and D'Mello [8], are used in the validation study. As previously presented by Ferreira et al [16], in the web-post resistance assessment, the finite element models can be validated against tests considering full beam and web-post models. The latter is a methodology consolidated in the literature and has been widely used by several researchers [7,9,16,28–34]. Geometrical and material nonlinear analysis with imperfections included (GMNIA) is considered. The initial geometric imperfection is applied with an amplitude of $d_g/500$, as recommended by Panedpojaman et al. [29], since it provided accurate results. A multilinear constitutive model of steel is employed, considering steel S355, as presented in Shamass and Guarracino [35] and Yun and Gardner [36]. The modulus of elasticity and Poisson's coefficient are equal to 200 GPa and 0.3, respectively. It is important to highlight that the development of full beams finite element models allows a comparison between the numerical and test results, i.e., load-displacement relationships. On the other hand, the web-post finite element model only allows numerical validation against test models considering the global shear.

3.1. Full models

Full models of perforated steel beam are modelled, considering 10 mm four-nodes S4R shell elements [16,37–39]. It has four nodes, six degrees of freedom (three rotations and three translations) per node and reduced integration, a factor that reduces processing time. The boundary conditions of the full models were applied according to Ferreira et al. [16]. According to the authors, simply supported beams with lateral restraint at the supports are considered. At the bottom of the stiffener in one end, vertical and longitudinal displacements are restrained (Uy=Uz=0). At the bottom of the stiffener in the other end, only the vertical displacement is restrained (Uy=0). At both ends, in the region of the stiffeners, lateral displacement and the rotation around the longitudinal axis are restrained at four points (Ux=URz=0) [16].

The validation results are presented considering load-displacement relationship (**Fig. 3**), as well as the final configuration (**Fig. 4**). According to the illustrations, it can be verified that the numerical models are validated.

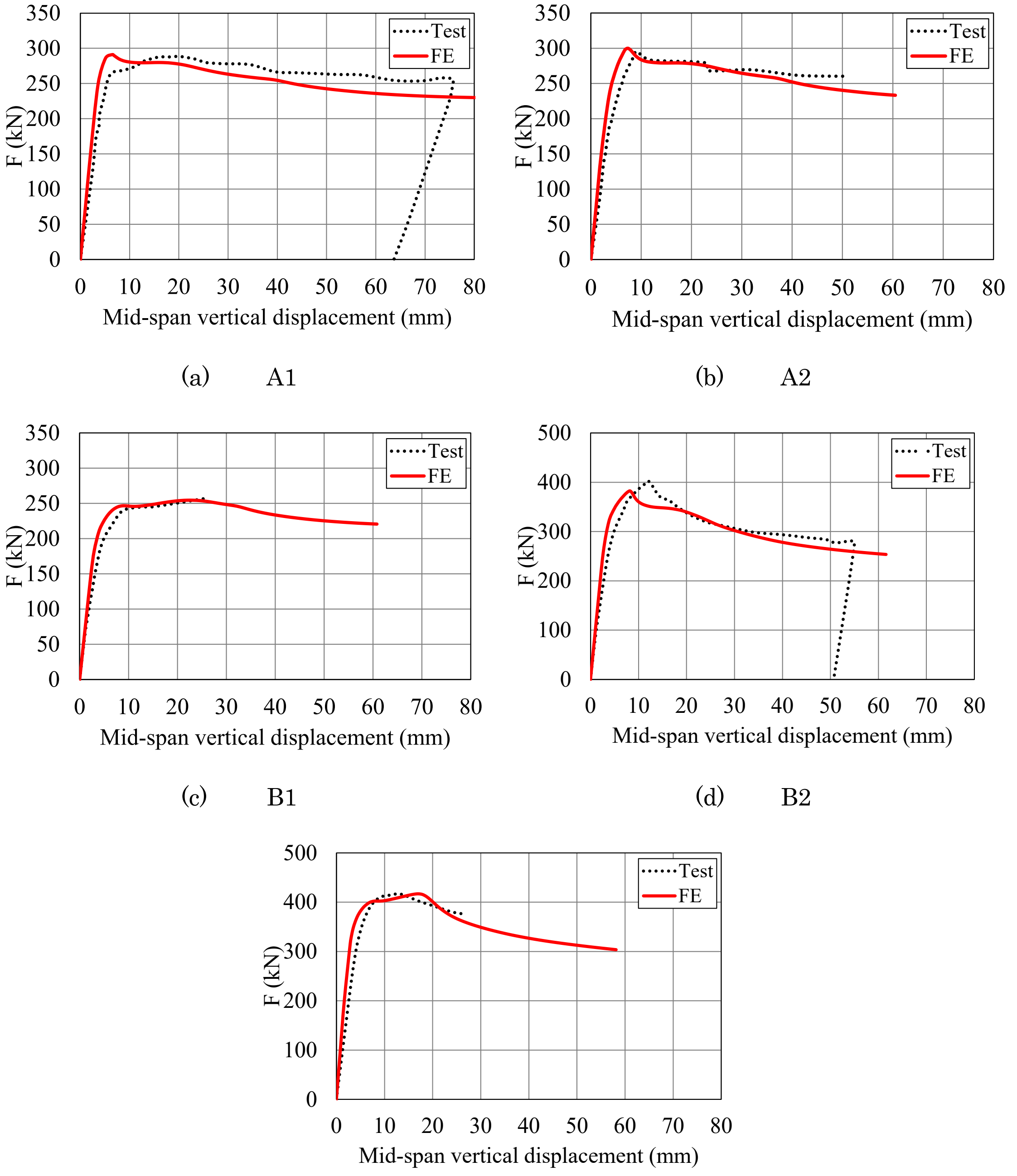

(a) A1

(b) A2

(c) B1

(d) B2

(e) B3

Fig. 3: Comparison between tests and finite element models by load-displacement relationships

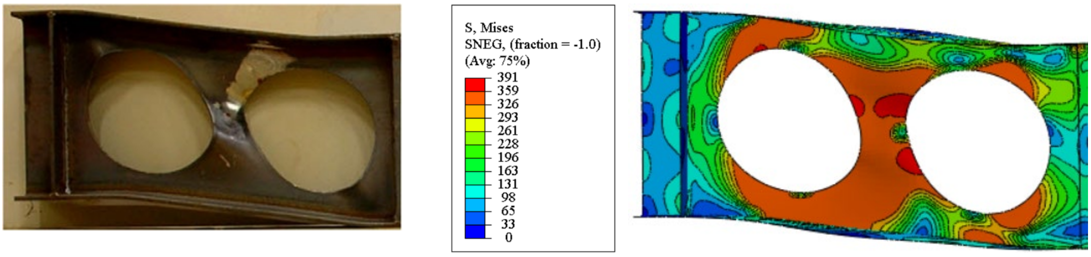

(a) A1

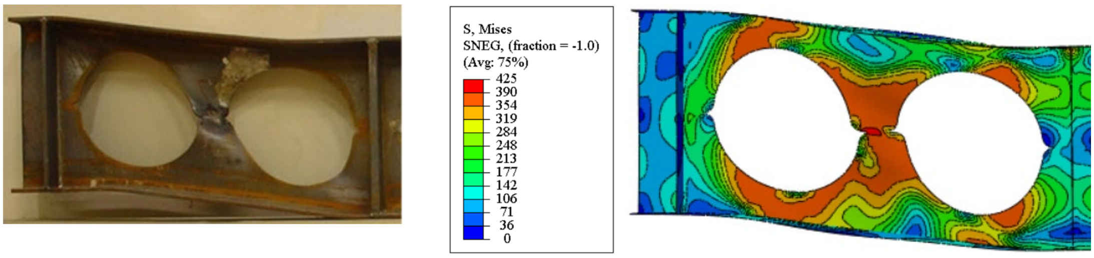

(b) A2

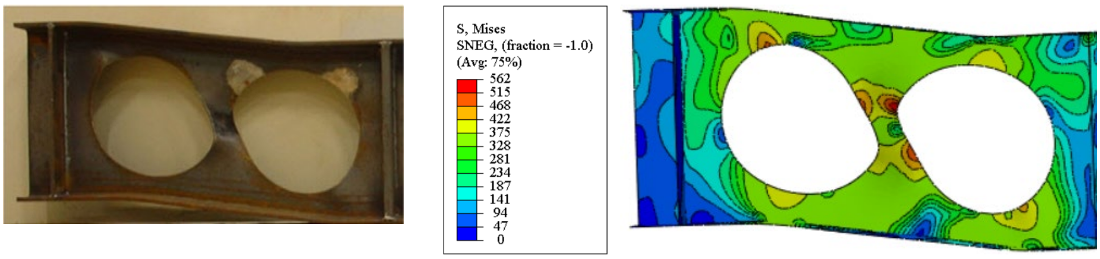

(c) B1

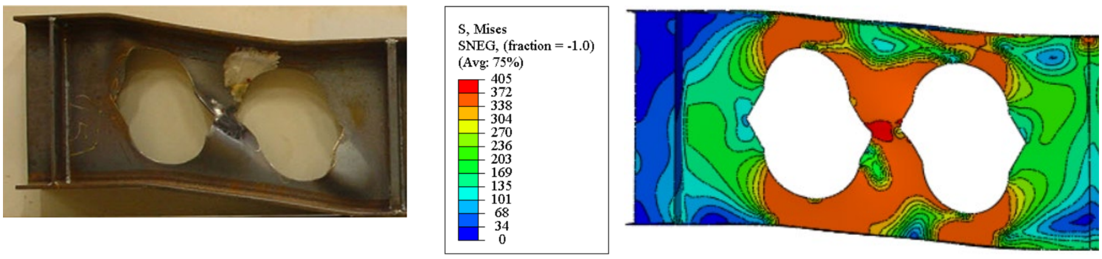

(d) B2

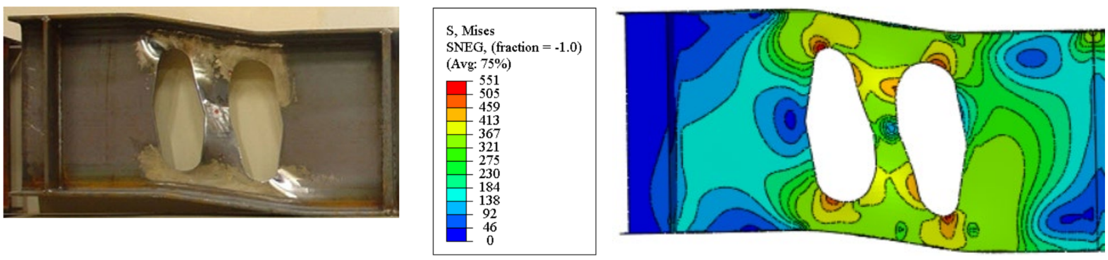

(e) B3

Fig. 4: Comparison between tests [8] and finite element models [16] by final configuration

3.2. Web-post models

Also, the web-post of a perforated steel beam is modelled, considering S4R shell elements. After several trials and comparisons with the tests results, the boundary conditions shown in **Fig. 5** were employed, resulting in adequate predictions. Shear loads were applied along the webs on the tee sections.

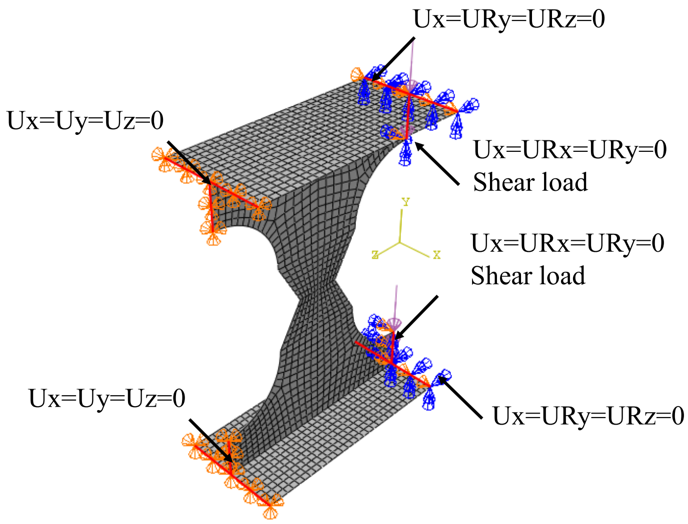

Fig. 5: Boundary conditions

The numerical model results, in comparison with the tests, are presented in **Fig. 6**. The maximum relative error was 9.4%. The standard deviation and variance were 6.93% and 0.48%, respectively. In this context, it is possible to state that the web-post finite element models were adequately validated. As the main concern of this paper is to investigate the web-post buckling resistance, a single web-post model is used.

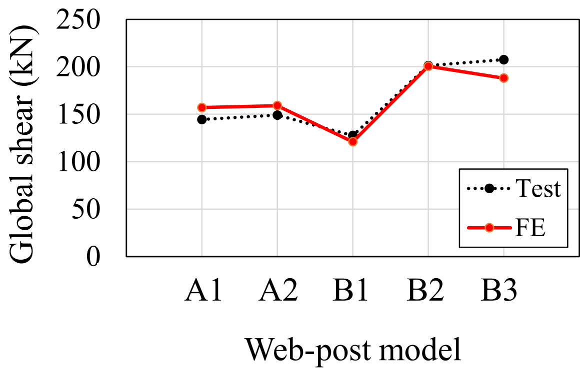

Fig. 6: Validation results of web-post models

4. Parametric study

The parametric study presented herein is based on the finite element validation study described in the previous section. The frequency in function of the investigated key parameters is illustrated in **Fig. 7**, in particular the flange width (**Fig. 7a**), the flange thickness (**Fig. 7b**), the distance between flanges geometric centres after castellation process (**Fig. 7c**), the web thickness (**Fig. 7d**), the opening height (**Fig. 7e**), the opening width (**Fig. 7f**), the opening radius (**Fig. 7g**) and high-strength steel grades (**Fig. 7h**). In total 13,500 finite element models are processed, taking into account the key parameters as illustrated in **Fig. 1**. The mean and coefficient of variation of each investigated parameter is presented in Table 1.

Table 1: Statistical analysis of geometric parameters

Geometrical parameter	Mean	Coefficient of variation
b_f (mm)	185.9	0.42
t_f (mm)	17.8	0.51
H (mm)	656.1	0.42
t_w (mm)	11.1	0.44
d_o (mm)	508.5	0.44
w (mm)	262.7	0.51
R (mm)	84.7	0.60

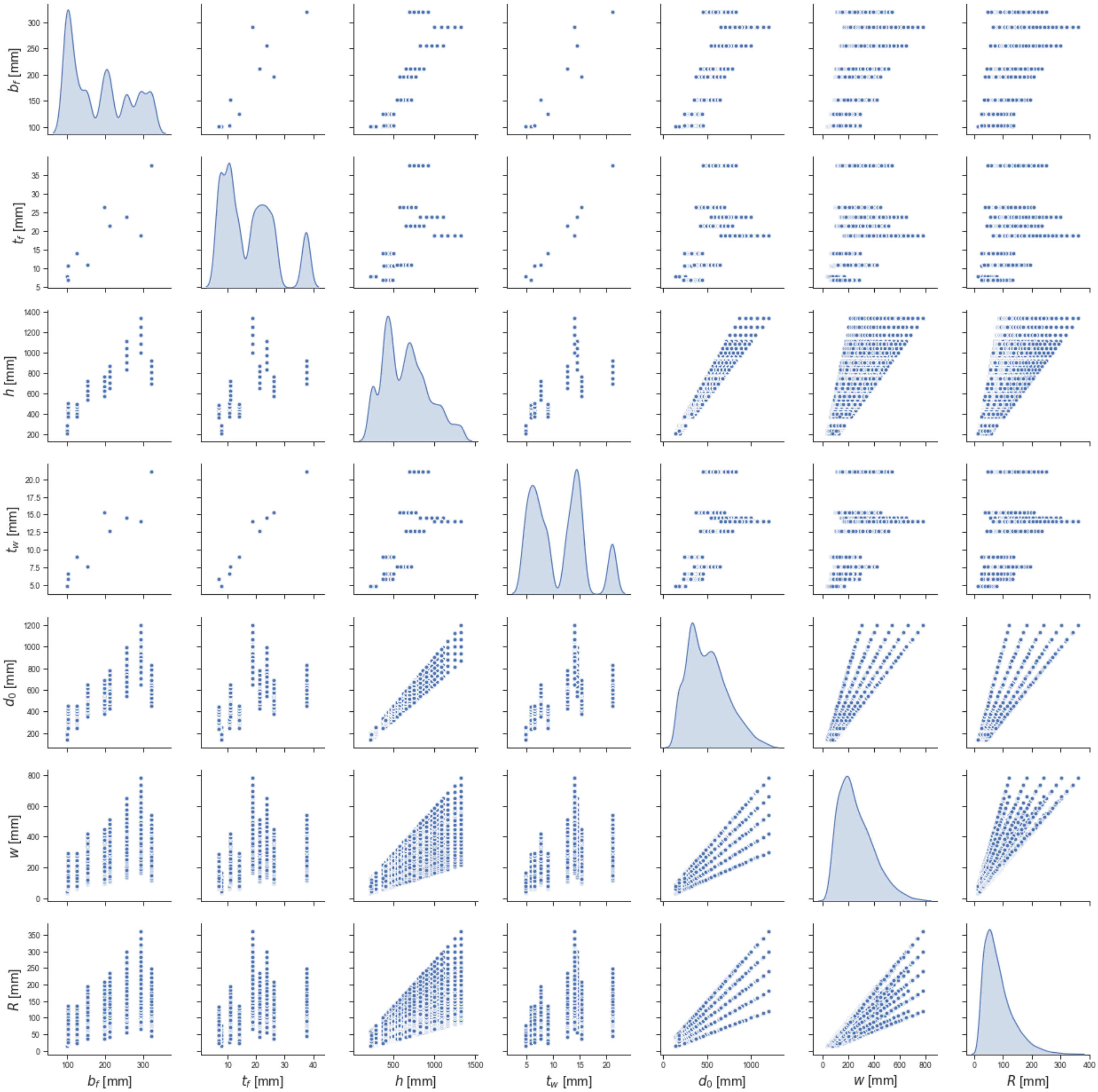

Fig. 7: Frequency based on parameters investigated

The models in the present parametric study include an eigenvalue buckling analysis followed by a geometrically nonlinear analysis with imperfections sympathetic with the first buckling mode and an imperfection size of $d_g/500$. The geometric nonlinear analysis including imperfections determines the web-post buckling mode and attains the capacity of the model. A Python script is developed to conduct the parametric study and post-process the results and it is available at https://github.com/luisantos090/WPB.

The script creates a finite element model according to the parameters in **Fig. 1** and the boundary conditions shown in **Fig. 5**. The mesh size discretises the web with 200 elements over the height and the flanges with 20 elements over the width. For the largest sections presented in this study, the mesh sizes are 6.7 and 14.6 mm for web and flanges, respectively. The web mesh size follows the recommendation of using 10 mm or less based on mesh sensitivity studies referenced previously in the validation study. The script post-processes the models by storing both the buckling load and the failure mode which are then used to develop and test the proposed new factor for web-post buckling of high-strength steels.

5. Results and discussion

Some examples of the finite element results that are normalised to the EC3 buckling curves and presented by Ferreira et al. [16] (**Eqs. 11-14**) are presented in **Figs. 8-11**, considering the variation of the key geometric parameters, as well the yield strength, in which $V_{cr,FE}$ and $V_{u,FE}$ are the global shear predicted by buckling and post-buckling analyses, respectively. From

13,500 finite element models processed, 10,764 models had the resistance defined by web-post buckling. As the influence of geometric parameters on capacity has already been discussed in Ferreira et al. [16] considering S355 steel grade, in this section only the analyses referring to high-strength steels are examined. In this way, the influence of yield strength on web-post buckling resistance of perforated steel beams with elliptically-based web openings is discussed briefly considering the key geometric parameters.

$$f_{cr,w,FE} = \frac{V_{cr,FE}}{t_w(s-w)} \tag{11}$$

$$\lambda_{0,FE} = \sqrt{\frac{f_y}{f_{cr,w,FE}}} \tag{12}$$

$$\sigma_{u,FE} = \frac{V_{u,FE}}{t_w(s-w)} \tag{13}$$

$$\chi_{FE} = \frac{\sigma_{u,FE}}{f_y} \tag{14}$$

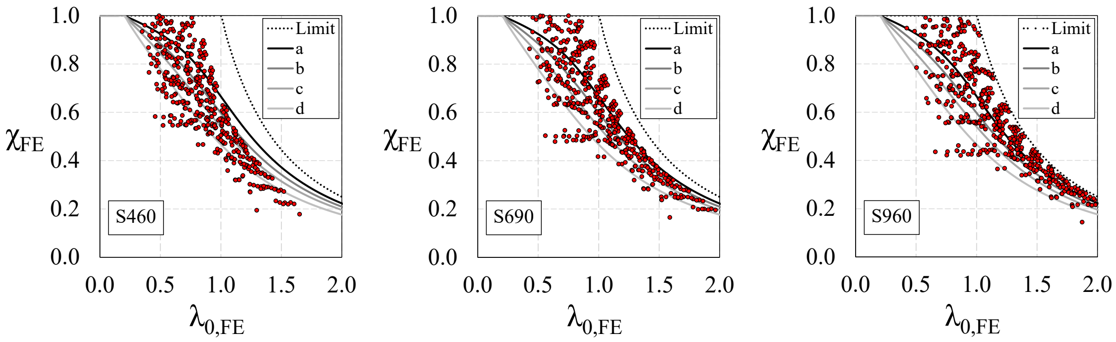

(a) *H*/*d*=1.2

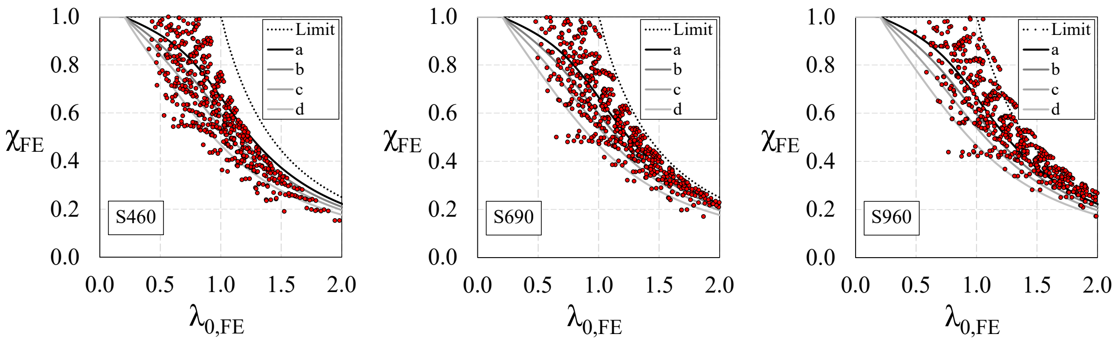

(b) *H*/*d*=1.4

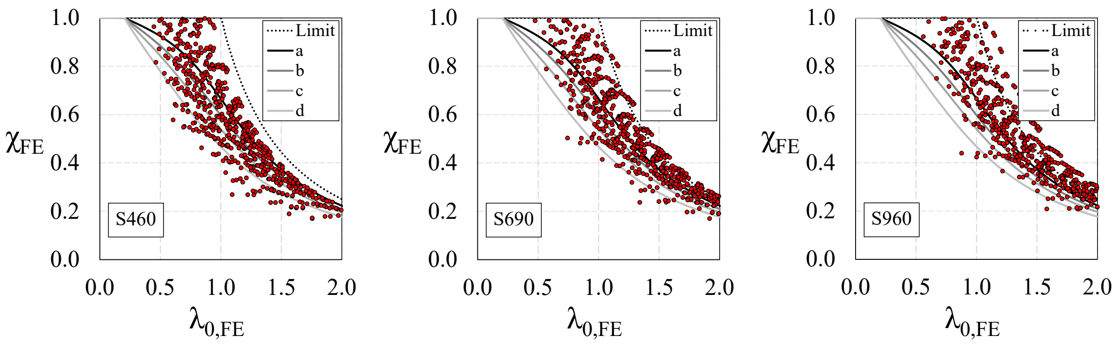

(c) *H*/*d*=1.6

Fig. 8: *H*/*d* ratio vs. buckling curves of EC3

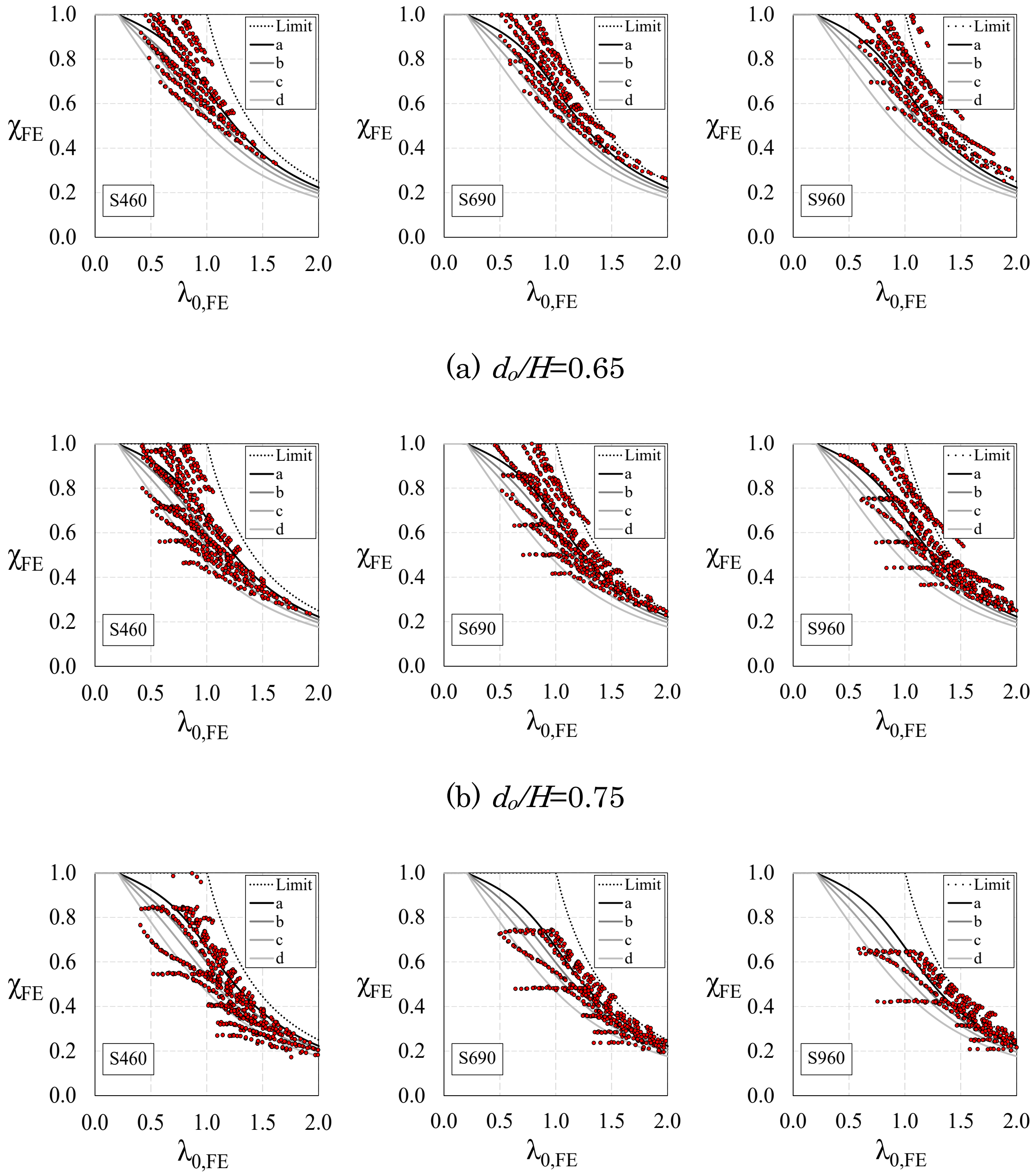

(a) d_o/H=0.65

(b) d_o/H=0.75

(c) d_o/H=0.85

Fig. 9: d_o/H ratio vs. buckling curves of EC3

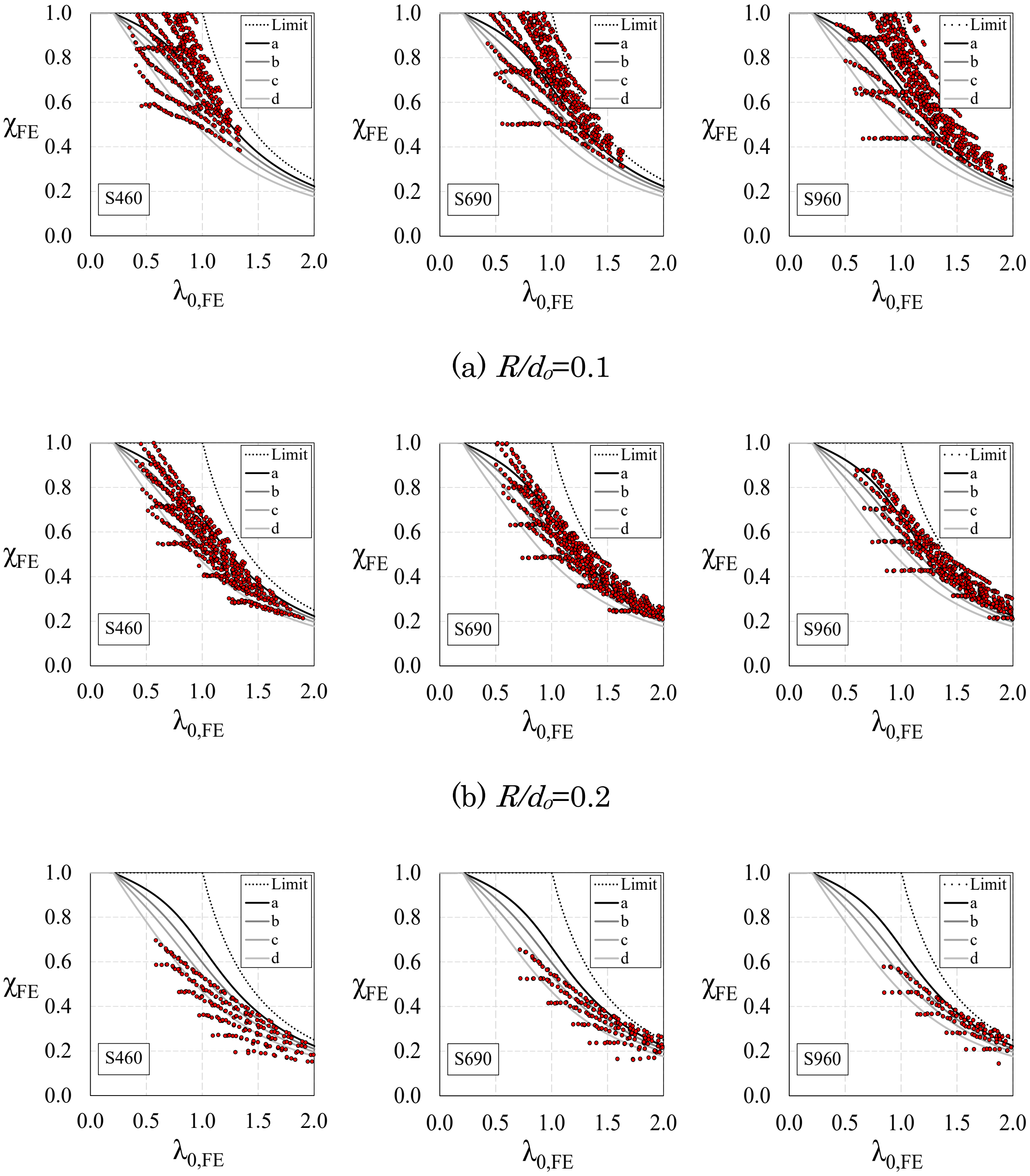

(a) R/d_o=0.1

(b) R/d_o=0.2

(c) R/d_o=0.3

Fig. 10: R/d_o ratio vs. buckling curves of EC3

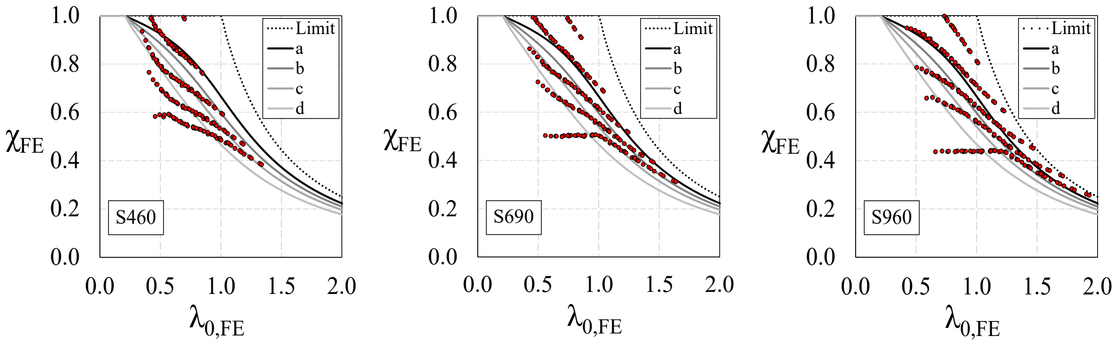

(a) w/d_o=0.25

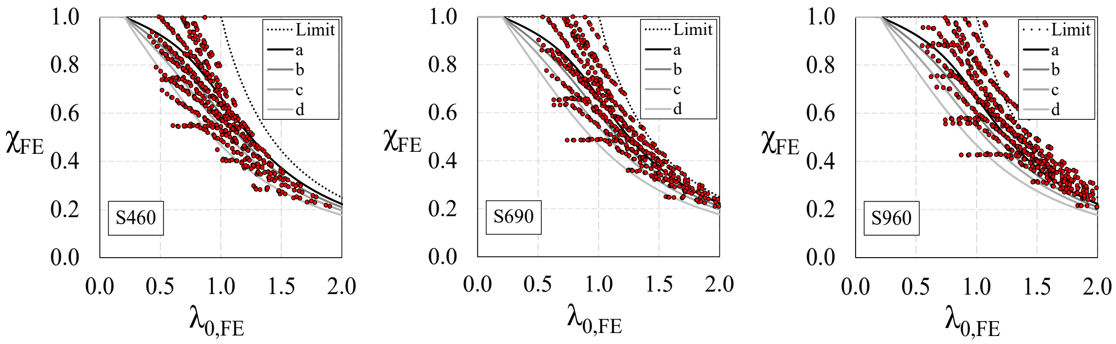

(b) w/d_o=0.45

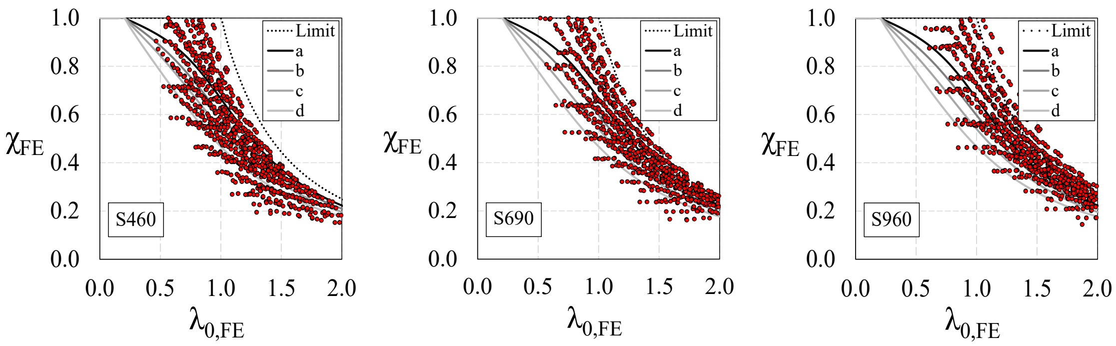

(c) w/d_o=0.65

Fig. 11: w/d_o ratio vs. buckling curves of EC3

5.1 *Yield strength*

From the analyses carried out, it was possible to observe the influence of the yield strength on the web-post buckling resistance. **Fig. 12** illustrates this behaviour, considering 1,200 data points, as an example. It is notable that the greater the yield strength, the greater the web-post buckling resistance. In this context, a comparative analysis can be made through the ratios V_{S690}/V_{S460}, V_{S960}/V_{S460}, and V_{S960}/V_{S690} considering the capacity of all finite element models. The S690 steel grade in relation to the S460 showed a minimum and maximum gain in capacity of 11% and 49%, respectively, with the average value of the V_{S690}/V_{S460} equal to 1.33. Regarding S960 steel grade compared to the S460, showed 24% and 99%, respectively, of a minimum and maximum gain in capacity. The average value of the V_{S960}/V_{S460} is equal to 1.61. Finally, by comparing the S960 and S690 steel grades, a minimum and maximum gain in capacity of 1% and 57%, respectively, was observed. The average value of the V_{S960}/V_{S690} is equal to 1.21.

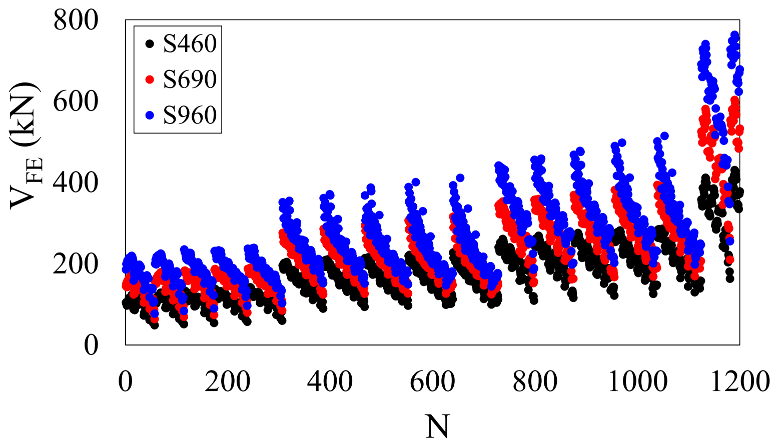

Fig. 12: Capacity of the web-post made of high-strength steels

5.2 *H/d* ratio

Fig. 13 provides the relationship between global shear capacity and *H/d* ratio for three classes of high-strength steel (S460, S690 and S960). The *H/d* ratio was increased from 1.2 to 1.6 in increments of 0.1. **Fig. 13a**, **Fig. 13b**, **Fig. 13c** and **Fig. 13d** show the impact of b_f, t_f and t_w, as parameters increase, there is an increase in resistance. Furthermore, it shows that as the expansion factor increases, so does the global shear capacity for all strength classes examined. When increasing the *H/d* ratio and keeping the other geometric parameters constant, there was an increase in global shear resistance. This can be explained by the increase in the steel area.

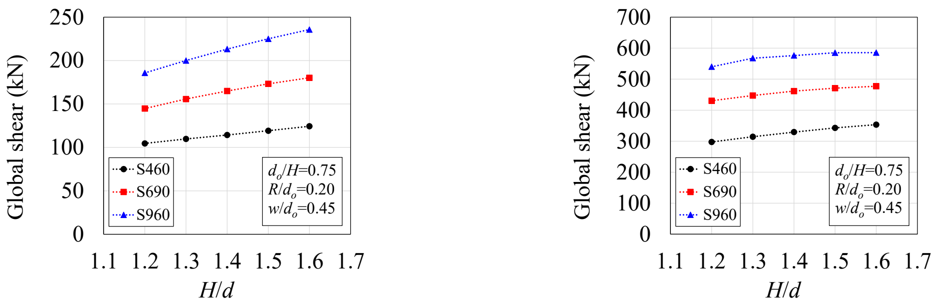

(a) b_f=101.2; t_f=7.9; t_w=4.8 (b) b_f=125.3; t_f=14.0; t_w=9.0

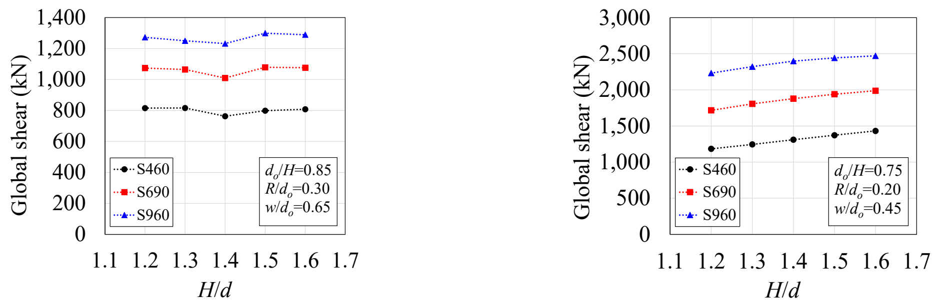

(c) b_f=255.8; t_f=23.7; t_w=14.5 (d) b_f=291.7; t_f=18.8; t_w=14.0

Fig. 13: Influence of *H/d* ratio on capacity (dimensions in mm)

Fig. 8 provided the EC3 buckling curves, and shows how the increase in the expansion ratio results in samples exceeding the resistance limit values. The impact of increasing the ratio of opening height over the distance between flanges geometric centres after the castellation process (d_o/H), the ratio of opening radius over opening height (R/d_o) and the ratio of opening width over opening height (w/d_o) can be seen in **Fig. 13c**. The trend showed a slight decrease in global shear capacity as the expansion factor increased from 1.2 to 1.4, thereafter, an increase in global shear capacity from 1.4 to 1.6. It can be assumed an increase in d_o and R will increase d_o/H and R/d_o respectively, therefore, decreasing the height of the tee section and decreasing the resistance to global shear capacity.

5.3 d_o/H ratio

Fig. 14 provides the relationship between global shear capacity and the ratio of opening height over the distance between flanges geometric centres after the castellation process (d_o/H) for the three classes of high-strength steel (S460, S690 and S960). Results clearly show that an increase in d_o/H will reduce the global shear capacity. This is due to the reduction in height of the tee section as stated in section 5.2. Furthermore, when reviewing **Fig. 9**, which provides d_o/H ratio vs. buckling curves of EC3, it can be seen that as d_o/H increases there is a decrease in capacity resistance. It also showed similar trends noted by Ferreira et al. [16], in which tee sections experienced instability phenomena before reaching the yield strength for d_o/H ratios of 0.75 and 0.85 and $\lambda_0 < 1.0$.

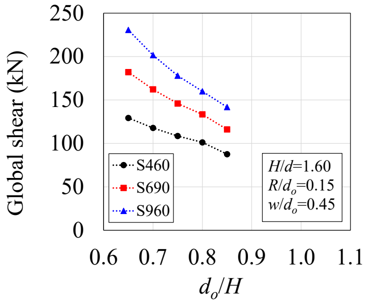

(a) *bf=101.2; tf=7.9; tw=4.8*

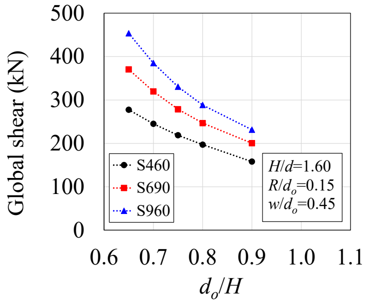

(b) b_f=102.4; t_f=10.8; t_w=6.6

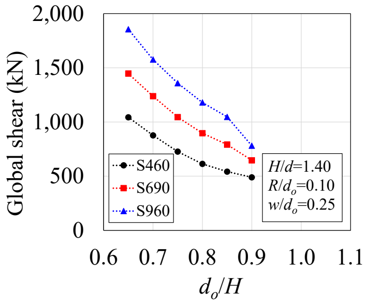

(c) b_f=196.7; t_f=26.3; t_w=15.3

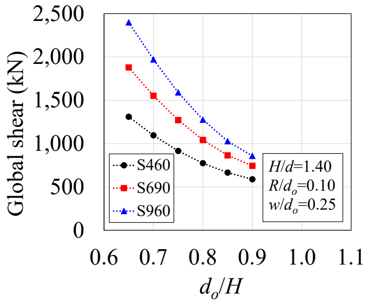

(d) b_f=291.7; t_f=18.8; t_w=14.0

Fig. 14: Influence of d_o/H ration on capacity (dimensions in mm)

5.4 *R/d*

The relationship between the global shear capacity and the ratio of opening radius over opening height *(R/d_o)* can be seen in **Fig. 15**, for the three classes of high-strength steel (S460, S690 and S960). R/d_o increased from 0.1 to 0.3 in increments of 0.5. **Fig. 15a** and **Fig. 15b** show that as the ratio increases to 0.15, there is a slight increase in the global shear, thereafter, as the ratio increases the capacity decreases. A similar trend can be noted in **Fig. 15b**. **Fig. 15c** shows that there is a negative relationship followed by a positive correlation. This shows that the beams are potentially sensitive to an increase in d_o/H.

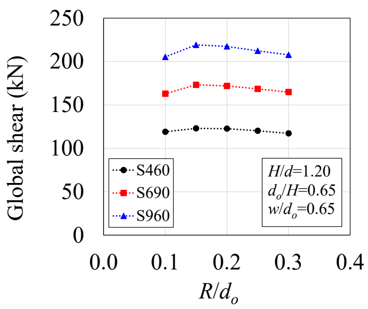

(a) *bf=101.2; tf=7.9; tw=4.8*

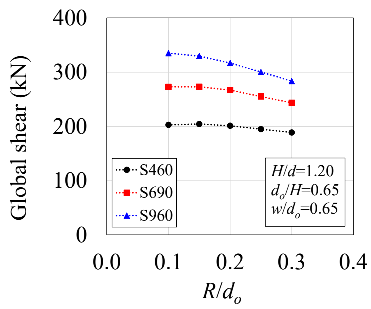

(b) b_f=101.6; t_f=7.0; t_w=5.8

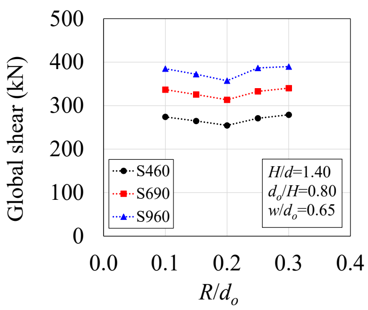

(c) b_f=152.4; t_f=10.9; t_w=7.6

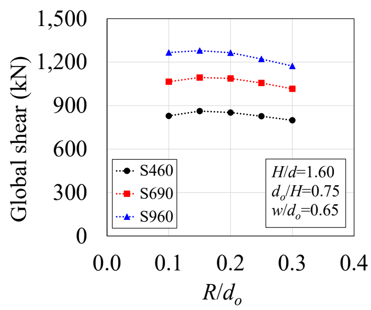

(d) b_f=320.2; t_f=37.6; t_w=21.1

Fig. 15: Influence of R/d_o ration on capacity (dimensions in mm)

As expected, as the opening radius increases so does R/d_o, resulting in a decreased resistance. However, from **Fig. 10** which provided R/d_o vs buckling curves for EC3, it is observed that the global shear is sensitive to R/d_o. As R/d_o is increased from 0.1 to 0.3, the resistance moves from exceeding the limit value to falling below or close to buckling curves *d* and *c*, respectively. Furthermore, it can be concluded that tee sections experienced instability phenomena before reaching the yield strength for R/d_o ratios of 0.1, 0.2 and 0.3 at $\lambda_0 < 1.0$, λ_0<1.75 and λ_0<2.0, respectively.

5.5 w/d_o ratio

Fig. 16 provides the relationship between global shear capacity and the ratio of opening width over opening height *(w/d_o)* for three classes of high-strength steel (S460, S690 and S960). Results show that an increase in w/d_o

increases the global shear. This is further verified by **Fig. 11**, which shows that as w/d_o increases, the resistance moves closer to exceeding the limits of the buckling curves of EC3.

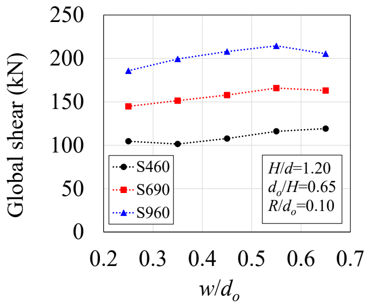

(a) *bf=101.2; tf=7.9; tw=4.8*

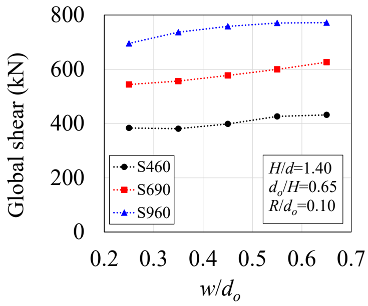

(b) b_f=125.3; t_f=14.0; t_w=9.0

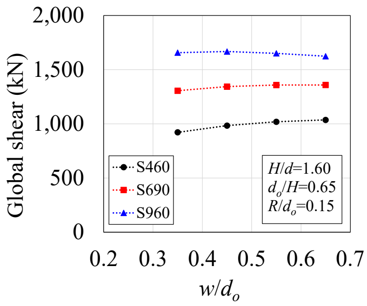

(c) b_f=211.9; t_f=21.3; t_w=12.7

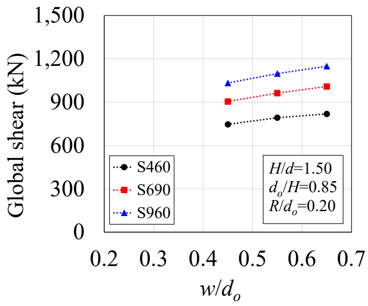

(d) b_f=291.7; t_f=18.8; t_w=14.0

Fig. 16: Influence of w/d_o ration on capacity (dimensions in mm)

6. Comparison with design equations for normal strength steel

In this section, the results of the finite element models are compared with the equation previously proposed by Ferreira et al. [16], considering normal strength steels (**Eqs. 1-10**), as shown in **Fig. 17**. In Appendix A an example of verification is shown. On analysis of the V_{FE}/V_{Rk} ratio as a comparison parameter, values of 0.88, 6.99% and 0.49% were verified for the S460 class, considering the average, standard deviation and variance, respectively. The maximum relative error was 33.71%, while the minimum relative error was -19.05%. In relation to the S690 class, the statistical values presented for the average, standard deviation and variance were, respectively, equal to 0.78, 8.52% and 0.73%. In this context, the maximum and minimum relative errors were equal to 46.1% and -13.34%. Finally, in relation to the S960 class, the average, standard deviation and variance values were equal to 0.70, 9.31% and 0.87%, respectively, and the maximum and minimum relative errors were equal to 55.29% and -7.34%. **Table 2** shows the statistical values, considering the general analysis.

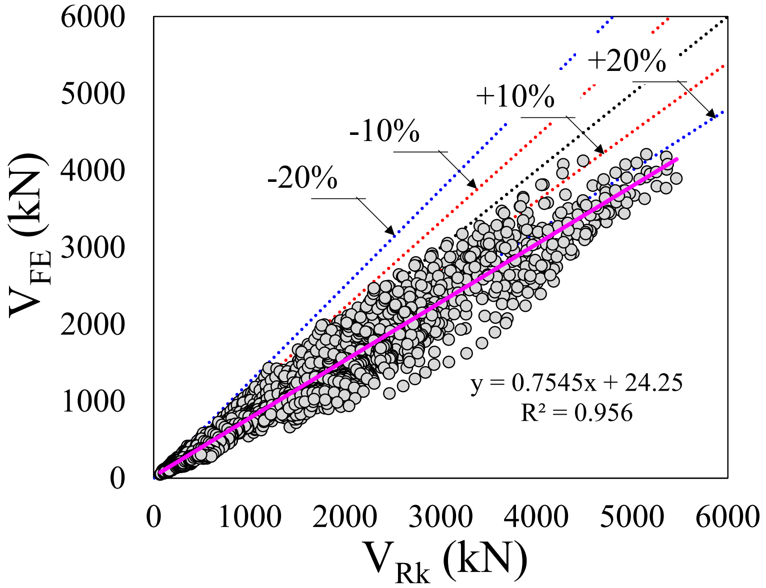

Fig. 17: FEM vs. Design equation for common strength steels

Table 2: Statistical analysis for design equation for normal strength steels

Analysis	**Value**
R^2 (Regression)	0.9560
RMSE (Root Mean Square Error) (kN)	99.5767
MAE (Mean Absolute Error) (kN)	73.2603
Minimum relative error	-16.00
Maximum relative error	123.70
Average (FEM/Predicted)	0.791
S.D.	11.20%
Var.	1.25%

7. Design recommendation

The calculation procedure proposed previously by Ferreira et al. [16] considered normal strength of steels. In this context, to adapt the high-strength steel models in the calculation of the web-post buckling resistance (**Eqs. 1-10**), a K_{HSS} factor is proposed, according to **Eqs (13-14)**. **Fig. 18** and **Table 3** show the statistical analysis with the application of the new factor. With this, it is possible to affirm that the new proposal presented is applicable for HSS. In the next section, a reliability analysis is applied according to Annex D EN 1990 [40]. It is worth to note that the coefficients of the **Eq. (14)** are obtained from the statistical analysis, hence, the proposed equation is limited to the geometric parameters illustrated in **Table 4** and **Fig. 19**.

$$\sigma_{Rk} = K_{HSS}\chi f_y \tag{13}$$

$$K_{HSS} = -1.45 + 1.61\left(\frac{H}{d_o}\right) + 0.33\left(\frac{s}{s-w}\right) - 0.90\left(\frac{s}{d_o}\right) + 0.21\left(\frac{w}{d_o}\right) - 0.004\left(\frac{d_o}{t_w}\right) + 0.49\lambda_0 \tag{14}$$

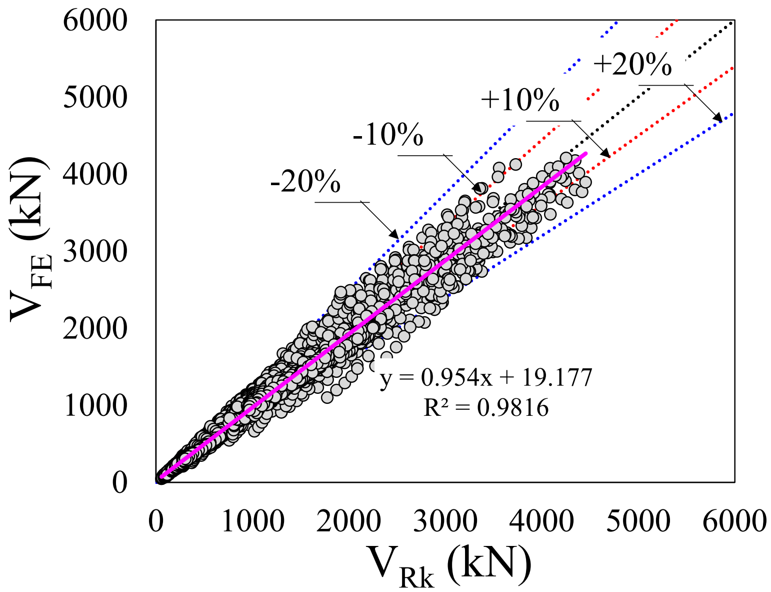

Fig. 18: FEM vs. Design equation for high-strength steel

Table 3: Statistical analysis for design equation for high-strength steel

Analysis	**Value**
R^2 (Regression)	0.9816
RMSE (Root Mean Square Error) (kN)	59.2871
MAE (Mean Absolute Error) (kN)	35.9576
Minimum relative error	-22.51
Maximum relative error	61.03
Average (FEM/Predicted)	0.985
S.D.	8.29%
Var.	0.69%

Table 4: Parameters limitation (in mm and MPa)

Parameter	**Minimum**	**Maximum**
Flange width (b_f)	101.2	320.2
Flange thickness (t_f)	7.0	37.6
Distance between flanges geometric centres (H)	213.4	1335.8
Web thickness (t_w)	4.8	21.1
Opening height (d_o)	138.7	1202.3
Opening width (w)	34.7	781.5
Opening radius (R)	13.9	360.7
Yield strength (f_y)	460	960

8. A statistical evaluation based on Annex D EN 1990

In this section, a statistical analysis based on Annex D EN 1990 (2002) [40] has been conducted to assess the reliability of the proposed formulation and propose a partial safety factor for web-post buckling resistance. The statistical evaluation of the proposed prediction model is done herein based on the generated numerical results.

Table 5 illustrates the key statistical parameters, including the number of data, n, the design fractile factor (ultimate limit state), $k_{d,n}$, the average ratio of numerical to resistance model predictions based on the least squares fit to the data, $\bar{b}$, the combined coefficient of variation incorporating both resistance model and basic variable uncertainties, V_r, and the partial safety factor for WPB resistance γ_{M0}. The COV of geometric properties and the high-strength steel material properties were assumed equal to 0.02 and 0.0055 [35]. The material over-strength of high-strength steel was taken equal to 1.135 [35]. The COV between the experimental and the numerical results, which was equal to 0.0133, was also considered. Performing First Order Reliability Method (FORM) in accordance with the Eurocode target reliability requirements, the partial factors γ_{M0} were evaluated. For S460, S690 and S960 the partial factors γ_{M0} were 1.03, 1.05 and 1.09, respectively. Furthermore, considering all HSS grades used in this study, the partial factor was 1.07.

Table 5: Summary of the reliability analysis for the proposed formulation

Grade	n	$\bar{b}$	$k_{d,n}$	V_r	γ_{M0}
S460	3588	1.013	3.04	0.102	1.03
S690	3588	0.994	3.04	0.102	1.05
S960	3588	0.961	3.04	0.103	1.09
All	10764	0.98	3.04	0.104	1.07

Concluding remarks

This paper is the first study of high-strength steel perforated steel beams with elliptically-based web openings. In particular, the web-post buckling is studied, and a resistance equation based on the truss model according to EUROCODE 3 is presented. A comprehensive parametric study of 13,500 FE models is carried out, considering the key geometric parameters that influence the web-post buckling resistance. A reliability analysis is also presented based on Annex D EN 1990 (2002). The following concluding remarks are summarised as:

1. The yield strength influenced the web-post buckling resistance. It was found that the greater the yield strength, the greater the web-post buckling resistance.
2. As the expansion factor (*H/d* ratio) increases, the global shear capacity for all three strength classes increases because of the increased in the steel area and therefore an increase in global shear resistance.
3. Decreasing the height of the tee section, so does the resistance to global shear capacity.
4. As the web opening radius increases, the R/d_o also increases, resulting in a decreased resistance. However, the global shear is sensitive to R/d_o.
5. The increase in w/ d_o increases the global shear. As w/d_o increases, the resistance moves closer to exceeding the limits of the buckling curves of EC3.

Appendix A: Application example

Check the web-post buckling resistance of perforated high-strength steel beams with elliptically-based web openings made of S460 and UB 457x152x52 section, considering the formulation for common and high-strength steel. Table A.1 presents the geometric characteristics of the section after the castellation process.

Table A.1: geometric characteristics

b_f (mm): 152.40	t_w (mm): 7.60	R (mm): 105.25
t_f (mm): 10.90	d_o (mm): 526.27	s (mm): 499.95
H (mm): 584.74	w (mm): 289.45	

For common steel:

- Web-post effective length and slenderness factor (Eqs 1-3):

$$k = 0.516 - 0.288\left(\frac{H}{d_o}\right) + 0.062\left(\frac{s}{s-w}\right) + 2.384\left(\frac{s}{d_o}\right) - 2.906\left(\frac{w}{d_o}\right)$$

$$\rightarrow k = 0.516 - 0.288\left(\frac{584.74}{526.27}\right) + 0.062\left(\frac{499{,}95}{499{,}95 - 289.45}\right) + 2.384\left(\frac{499{,}95}{526.27}\right)$$

$$- 2.906\left(\frac{289.45}{526.27}\right)$$

$$\rightarrow k = 1.01$$

Thus:

$$l_{eff} = k\sqrt{\left(\frac{d_o - 2R}{2}\right)^2 + \left(\frac{s}{2} - R\right)^2}$$

$$\rightarrow l_{eff} = 1.01\sqrt{\left(\frac{526.27 - 2 \times 105.25}{2}\right)^2 + \left(\frac{499{,}95}{2} - 105.25\right)^2}$$

$$\rightarrow l_{eff} = 216.26 \text{ mm}$$

Finally:

$$\lambda_w = \frac{l_{eff}\sqrt{12}}{t_w} = \frac{216.26\sqrt{12}}{7.60} 98.57$$

- EC3 reduction factor (Eqs 4-7):

Critical shear stress in the web-post:

$$f_{cr,w} = \frac{\pi^2 E}{{\lambda_w}^2} = \frac{\pi^2 \times 200000}{98.57^2} = 203.15\ MPa$$

The reduced slenderness factor:

$$\lambda_0 = \sqrt{\frac{f_y}{f_{cr,w}}} = \sqrt{\frac{460}{203.15}} = 1.50$$

Imperfection factor:

$$\phi = 0.5\left[1 + 0.49(\lambda_0 - 0.2) + {\lambda_0}^2\right] = 0.5[1 + 0.49(1.50 - 0.2) + 1.50^2] = 1.95$$

Finally, the reduction factor

$$\chi = \frac{1}{\phi + \sqrt{\phi^2 - {\lambda_0}^2}} = \frac{1}{1.95 + \sqrt{1.95^2 - 1.50^2}} = 0.31$$

- Web-post buckling resistance (Eqs 8-10):

$$K = -1.318 + 1.790\left(\frac{H}{d_o}\right) + 0.413\left(\frac{s}{s-w}\right) - 1.926\left(\frac{s}{d_o}\right) + 0.937\left(\frac{w}{d_o}\right) - 0.02\left(\frac{d_o}{t_w}\right)$$

$$+ 1.412\lambda_0$$

$$\rightarrow K = -1.318 + 1.790\left(\frac{584.74}{526.27}\right) + 0.413\left(\frac{499{,}95}{499{,}95 - 289.45}\right) - 1.926\left(\frac{499{,}95}{526.27}\right)$$

$$+ 0.937\left(\frac{289.45}{526.27}\right) - 0.02\left(\frac{526.27}{7.6}\right) + 1.412 \times 1.50$$

$$\rightarrow K = 1.08$$

Thus, the ultimate stress can be calculated:

$$\sigma_{Rk} = K\chi f_y = 1.08 \times 0.31 \times 460 = 155.1\ MPa$$

Finally, the web-post buckling resistance is predicted:

$$V_{Rk} = \sigma_{Rk} t_w (s - w) = 155.1 \times 7.6(499{,}95 - 289.45) = 248.13\ kN$$

For high-strength steel:

The procedure is similar to that used in common steel, considering Eqs. (1-7) shown previously.

-Web-post buckling resistance (Eqs 13-14):

$$K_{HSS} = -1.45 + 1.61\left(\frac{H}{d_o}\right) + 0.33\left(\frac{s}{s-w}\right) - 0.90\left(\frac{s}{d_o}\right) + 0.21\left(\frac{w}{d_o}\right) - 0.004\left(\frac{d_o}{t_w}\right) + 0.49\lambda_0$$

$$\rightarrow K_{HSS} = -1.45 + 1.61\left(\frac{584.74}{526.27}\right) + 0.33\left(\frac{499,95}{499,95 - 289.45}\right) - 0.90\left(\frac{499,95}{526.27}\right) + 0.21\left(\frac{289.45}{526.27}\right) - 0.004\left(\frac{526.27}{7.6}\right) + 0.49 \times 1.50$$

$$\rightarrow K_{HSS} = 0.84$$

Thus, the ultimate stress can be calculated:

$$\sigma_{Rk} = K_{HSS}\chi f_y = 0.84 \times 0.31 \times 460 = 119.78\ MPa$$

Finally, the web-post buckling resistance is predicted:

$$V_{Rk} = \sigma_{Rk} t_w (s - w) = 119.78 \times 7.6(499,95 - 289.45) = 194.29\ kN$$

Table A.2 shows the comparison between the equations with the prediction of the finite element method.

Table A.2: Comparative analysis

Common steel method	High-strength steel method	Finite element method
248.13 kN	194.29 kN	205.81 kN

References

[1] F.P.V. Ferreira, C.H. Martins, S. De Nardin, Advances in composite beams with web openings and composite cellular beams, J Constr Steel Res. 172 (2020) 106182. https://doi.org/10.1016/j.jcsr.2020.106182.

[2] R.M.M. Lawson, J. Lim, S.J.J. Hicks, W.I.I. Simms, Design of composite asymmetric cellular beams and beams with large web openings, J Constr Steel Res. 62 (2006) 614–629. https://doi.org/10.1016/j.jcsr.2005.09.012.

[3] F.P.V. Ferreira, R. Shamass, V. Limbachiya, K.D. Tsavdaridis, C.H. Martins, Lateral–torsional buckling resistance prediction model for steel cellular beams generated by Artificial Neural Networks (ANN), Thin-Walled Structures. 170 (2022) 108592. https://doi.org/10.1016/j.tws.2021.108592.

[4] E. Ellobody, Nonlinear analysis of cellular steel beams under combined buckling modes, Thin-Walled Structures. 52 (2012) 66–79. https://doi.org/10.1016/j.tws.2011.12.009.

[5] K.M. El-Sawy, A.M.I. Sweedan, M.I. Martini, Moment gradient factor of cellular steel beams under inelastic flexure, J Constr Steel Res. 98 (2014) 20–34. https://doi.org/10.1016/j.jcsr.2014.02.007.

[6] P. Panedpojaman, W. Sae-Long, T. Chub-Uppakarn, Cellular beam design for resistance to inelastic lateral-torsional buckling, Thin-Walled Structures. 99 (2016) 182–194. https://doi.org/10.1016/j.tws.2015.08.026.

[7] L.F. Grilo, R.H. Fakury, A.L.R. de Castro e Silva, G. de S. Veríssimo, Design procedure for the web-post buckling of steel cellular beams, J Constr Steel Res. 148 (2018) 525–541. https://doi.org/10.1016/j.jcsr.2018.06.020.

[8] K.D. Tsavdaridis, C. D'Mello, Web buckling study of the behaviour and strength of perforated steel beams with different novel web opening shapes, J Constr Steel Res. 67 (2011) 1605–1620. https://doi.org/10.1016/j.jcsr.2011.04.004.

[9] V. Limbachiya, R. Shamass, Application of Artificial Neural Networks for web-post shear resistance of cellular steel beams, Thin-Walled Structures. 161 (2021) 107414. https://doi.org/10.1016/j.tws.2020.107414.

[10] D. Kerdal, D.A. Nethercot, Failure modes for castellated beams, J Constr Steel Res. 4 (1984) 295–315. https://doi.org/10.1016/0143-974X(84)90004-X.

[11] K.D. Tsavdaridis, Structural performance of perforated steel beams with novel web openings and with partial concrete encasement, Doctoral Thesis, City University London, 2010. https://openaccess.city.ac.uk/id/eprint/11660/.

[12] K.D. Tsavdaridis, C. D'Mello, FE Investigation of Perforated Sections with Standard and Non-Standard Web Opening Configurations and Sizes, in: S.L. Chan (Ed.), 6th International Conference on Advances Is Steel Structures, Hong Kong Institute of Steel Construction, Hong Kong, China, 2009: pp. 213–220.

[13] K.D. Tsavdaridis, C. D'Mello, Vierendeel Bending Study of Perforated Steel Beams with Various Novel Web Opening Shapes through Nonlinear Finite-Element Analyses, Journal of Structural Engineering. 138 (2012) 1214–1230. https://doi.org/10.1061/(asce)st.1943-541x.0000562.

[14] K.D. Tsavdaridis, J.J. Kingman, V. V. Toropov, Application of structural topology optimisation to perforated steel beams, Comput

Struct. 158 (2015) 108–123. https://doi.org/10.1016/j.compstruc.2015.05.004.

[15] K.D. Tsavdaridis, C. D'Mello, Optimisation of novel elliptically-based web opening shapes of perforated steel beams, J Constr Steel Res. 76 (2012) 39–53. https://doi.org/10.1016/j.jcsr.2012.03.026.

[16] F.P.V. Ferreira, R. Shamass, L.F.P. Santos, V. Limbachiya, K.D. Tsavdaridis, EC3 design of web-post buckling resistance for perforated steel beams with elliptically-based web openings, Thin-Walled Structures. 175 (2022) 109196. https://doi.org/10.1016/j.tws.2022.109196.

[17] European committee for standardization, EN 1993-1-1: Eurocode 3 – Design of steel structures – Part 1-1: General rules and rules for buildings, (2002).

[18] K.D. Tsavdaridis, C. D'Mello, Structural beam, GB 2492176, 2012.

[19] C. Miki, K. Homma, T. Tominaga, High strength and high performance steels and their use in bridge structures, J Constr Steel Res. 58 (2002) 3–20. https://doi.org/10.1016/S0143-974X(01)00028-1.

[20] M. Veljkovic, B. Johansson, Design of hybrid steel girders, J Constr Steel Res. 60 (2004) 535–547. https://doi.org/10.1016/S0143-974X(03)00128-7.

[21] R. Bjorhovde, Development and use of high performance steel, J Constr Steel Res. 60 (2004) 393–400. https://doi.org/10.1016/S0143-974X(03)00118-4.

[22] A. WHEELER, B. RUSSELL, Behaviour and design of webs in high strength steel under flexural loading, in: Fourth International Conference on Advances in Steel Structures, Elsevier, 2005: pp. 137–142. https://doi.org/10.1016/B978-008044637-0/50018-4.

[23] G. Shi, X. Zhu, H. Ban, Material properties and partial factors for resistance of high-strength steels in China, J Constr Steel Res. 121 (2016) 65–79. https://doi.org/10.1016/j.jcsr.2016.01.012.

[24] B. Karabulut, G. Ferraz, B. Rossi, Lifecycle cost assessment of high strength carbon and stainless steel girder bridges, J Environ Manage. 277 (2021) 111460. https://doi.org/10.1016/j.jenvman.2020.111460.

[25] K. Mela, M. Heinisuo, Weight and cost optimization of welded high strength steel beams, Eng Struct. 79 (2014) 354–364. https://doi.org/10.1016/j.engstruct.2014.08.028.

[26] Dassault Systèmes Simulia, Abaqus 6.18, (2016).

[27] R.M. Lawson, S.J. Hicks, Design of composite beams with large web openings. SCI P355., The Steel Construction Institute, 2011.

[28] W. Zaarour, R. Redwood, Web Buckling in Thin Webbed Castellated Beams, Journal of Structural Engineering. 122 (1996) 860–866. https://doi.org/10.1061/(ASCE)0733-9445(1996)122:8(860).

[29] P. Panedpojaman, T. Thepchatri, S. Limkatanyu, Novel design equations for shear strength of local web-post buckling in cellular beams, Thin-Walled Structures. 76 (2014) 92–104. https://doi.org/10.1016/j.tws.2013.11.007.

[30] K.D. Tsavdaridis, G. Galiatsatos, Assessment of cellular beams with transverse stiffeners and closely spaced web openings, Thin-Walled Structures. 94 (2015) 636–650. https://doi.org/10.1016/j.tws.2015.05.005.

[31] S. Durif, A. Bouchaïr, O. Vassart, Experimental and numerical investigation on web-post specimen from cellular beams with sinusoidal openings, Eng Struct. 59 (2014) 587–598. https://doi.org/10.1016/j.engstruct.2013.11.021.

[32] F.P.V. Ferreira, K.D. Tsavdaridis, C.H. Martins, S. De Nardin, Ultimate strength prediction of steel–concrete composite cellular beams with PCHCS, Eng Struct. 236 (2021) 112082. https://doi.org/10.1016/j.engstruct.2021.112082.

[33] F.P.V. Ferreira, K.D. Tsavdaridis, C.H. Martins, S. De Nardin, Buckling and post-buckling analyses of composite cellular beams, Compos Struct. 262 (2021). https://doi.org/10.1016/j.compstruct.2021.113616.

[34] F.P.V. Ferreira, K.D. Tsavdaridis, C.H. Martins, S. De Nardin, Composite action on web-post buckling shear resistance of composite cellular beams with PCHCS and PCHCSCT, Eng Struct. 246 (2021) 113065. https://doi.org/10.1016/j.engstruct.2021.113065.

[35] R. Shamass, F. Guarracino, Numerical and analytical analyses of high-strength steel cellular beams: A discerning approach, J Constr Steel Res. 166 (2020) 105911. https://doi.org/10.1016/j.jcsr.2019.105911.

[36] X. Yun, L. Gardner, Stress-strain curves for hot-rolled steels, J Constr Steel Res. 133 (2017) 36–46. https://doi.org/10.1016/j.jcsr.2017.01.024.

[37] F.P.V. Ferreira, A. Rossi, C.H. Martins, Lateral-torsional buckling of cellular beams according to the possible updating of EC3, J Constr Steel Res. 153 (2019) 222–242. https://doi.org/10.1016/j.jcsr.2018.10.011.

[38] F.P.V. Ferreira, C.H. Martins, LRFD for Lateral-Torsional Buckling Resistance of Cellular Beams, International Journal of Civil Engineering. 18 (2020) 303–323. https://doi.org/10.1007/s40999-019-00474-7.

[39] R. Shamass, F.P.V. Ferreira, V. Limbachiya, L.F.P. Santos, K.D. Tsavdaridis, Web-post buckling prediction resistance of steel beams with elliptically-based web openings using Artificial Neural Networks (ANN), Thin-Walled Structures. 180 (2022) 109959. https://doi.org/10.1016/j.tws.2022.109959.

[40] European committee for standardization, EN 1990: Eurocode – Basis of structural design, (n.d.).